Title
Collision and composite tumors; radiologic and pathologic correlation.

Journal
Abdominal radiology (New York), 42(12)

ISSN
2366-004X

Authors
Sung, Calvin T
Shetty, Anup
Menias, Christine O
et al.

Publication Date
2017-12-01

DOI
10.1007/s00261-017-1200-x

Abdominal Radiology

Abdom Radiol (2017)
DOI: 10.1007/s00261-017-1200-x

Collision and composite tumors; radiologic and pathologic correlation

Calvin T. Sung,[1,2] Anup Shetty,[3] Christine O. Menias,[4] Roozbeh Houshyar,[1] Shreya Chatterjee,[1] Thomas K. Lee,[1] Paul Tung,[1] Mohammed Helmy,[1] Chandana Lall[1]

[1]Department of Radiological Sciences, Irvine School of Medicine, University of California, 101 The City Drive South, Suite #1105, Orange, CA 92868, USA
[2]School of Medicine, University of California Riverside, 900 University Ave., Riverside, CA 92521, USA
[3]Department of Radiology, Washington University School of Medicine in St. Louis, 510 South Kingshighway Boulevard, St. Louis, MO 63110, USA
[4]Department of Radiology, Mayo Clinic, Phoenix, AZ 85054, USA

Abstract

The terms composite and collision tumors have been used interchangeably throughout radiological literature. Both composite and collision tumors involve two morphologically and immunohistochemically distinct neoplasms coexisting within a single organ. However, collision tumors lack the histological cellular intermingling seen in composite tumors. Composite tumors often arise from a common driver mutation that induces a divergent histology from a common neoplastic source while collision tumors may arise from coincidental neoplastic change. The purpose of this review is to provide an overview of abdominal composite and collision tumors by discussing hallmark radiographic and pathological presentations of rare hepatic, renal, and adrenal case studies. A better understanding of the presentation of each lesion is imperative for proper recognition, diagnosis, and management of these unique tumor presentations.

Key words: Biphenotypic—Composite hepatocellular and cholangiocarcinoma—Live collision—Composite renal cell carcinoma—Collision cholangiocarcinoma—Renal collision—Adrenal collision

By definition, the term collision tumor refers to independently coexisting neoplasms with different behavioral, genetic, and histological features that are sharply demarcated and lack significant tissue admixture [1–3]. Composite tumors also comprised two morphologically and immunohistochemically distinct neoplasms coexisting within the proximity of the same organ; however, they have actual cellular intermingling and a common driver mutation that results in divergent histology from a common source [4, 5]. Although there is no consensus for defining synchronous tumors, they generally refer to two behaviorally and histologically distinct tumors that are physically separated but occur simultaneously or following each other in sequence by less than 2 months [6]. The presence of two different cell types can lead to perplexing imaging findings, which at times, makes the diagnosis of a collision or composite tumor challenging and may necessitate a biopsy for confirmation.

Currently there are three hypothesis regarding the pathogenesis of composite and collision tumors. The simplest, although not necessarily the most likely, explanation is the coincidental occurrence of two primary neoplasms within a common location. A second hypothesis suggests that a common carcinogenic stimulus may have altered the cellular microenvironment within the proximity of which two distinct neoplasms arise from. Similarly, the last hypothesis suggests that the first tumor may have altered the microenvironment within the organ and increased the likelihood of developing another primary tumor or facilitated metastatic seeding within the vicinity [7]. Composite and collision tumors are extremely rare, considering that only 63 cases of collision tumors were reported in 2015 [3]. While imaging alone may not be sufficient to diagnose the tumors involved, it is imperative to clinically recognize the duality of these lesions since the biopsy of only a single component may result in an incomplete diagnosis, suboptimal treatment, and adverse consequences. In the

Correspondence to: Chandana Lall; *email:* clall@uci.edu

Published online: 16 June 2017

following section, we will correlate the imaging findings and histopathology of composite and collision tumors of hepatobiliary, renal, and adrenal origins.

Hepatobiliary composite tumors

The co-existence of hepatocellular carcinomas (HCCs) and cholangiocarcinoma (CCs) is the most commonly described form of composite (combined or mixed) tumor according to literature, even though this type of lesion constitutes less than 1% of all HCCs [2, 8]. Hepatocellular cholangiocarcinomas (HCC–CCs) are primary liver composite carcinomas with biphenotypic differentiation that stem from either common progenitor cell lineages or the dedifferentiation of mature liver cells [9]. Studies indicate that HCC–CCs have a worse prognosis than either HCC or CC alone [10–16]. Treatment modalities include local radiofrequency ablative therapy, chemotherapy, transarterial chemoembolization, liver transplantation, and radical resection, which is preferred over nonoperative management in terms of survival outcome (16.5 months) [13, 15, 17, 18]. Approximately 20% of all liver transplants in the United States are performed for HCC, and current guidelines state that pathologic proof is not required if MRI and CT imaging with contrast is concordant [18, 19]. Before conducting invasive treatment prior to pathology, the findings that HCC–CC has a 78% 5-year recurrence rate compared to 17% in HCC patients should be considered in regards to the patient's prognosis despite the fact that HCC–CCs constitute less than 1% of all HCCs [9, 20].

Primary malignant liver tumors resemble and arise from major constituent liver cells [21]. For example, hepatocytes give rise to HCC, biliary epithelial cells to CC and biliary cystadenocarcinoma, and endothelial cells to angiosarcoma and epithelioid hemangioendothelioma [21]. When determining etiology, it should be noted that metastases outnumber primary liver malignant tumors 30–1 [21]. Composite HCC–CC is acknowledged as a distinct subtype of CC [22, 23]. World Health Organization (WHO) guidelines define HCC–CC as a tumor with unequivocal, intermixed elements of HCC and CC [19]. HCC–CC is subdivided into type A (separate foci of HCC and CC within the same liver lobe), type B (adjacent HCC and CC comingling with continued growth), and type C (components of HCC and CC within the same mass) according to the Allen and Lisa's classification scheme [9, 24]. Similarly, Goodman et al. categorized HCC–CC with type I tumors (HCC and CC within the same liver), type II (transition from elements of HCC to elements of CC), and type III (fibrolamellar tumors containing mucin-producing pseudoglands) [9, 24].

In terms of the individual tumors, HCC commonly develop in patients with chronic liver diseases including hepatitis B or C, aflatoxin exposure, steatohepatitis, hereditary hemochromatosis, and alpha-1-antitrypsin deficiency with or without cirrhosis, which is the greatest single risk factor for developing HCC [25]. CC is an adenocarcinoma that arises from the biliary epithelium due to parasitic infections, biliary duct cysts, and primary sclerosing cholangitis [26]. CCs are divided into intrahepatic (20%) and extrahepatic (80%) tumors based not only on anatomic location but also differences in their risk factors, clinical presentations, and therapies [27].

Detailed histopathologic evaluation with specific immunohistochemistry (IHC) markers is also critical in confirming the diagnosis of HCC–CC. Immunohistochemistry markers for HCC include CD 10, alpha-fetoprotein (αFP), cytoplasmic hepatocyte paraffin 1, and polyclonal CEA, while biliary markers for CC include the carbohydrate antigens keratin 7 and 19 [28, 29]. Although these tumor markers are not extremely specific or sensitive for HCC–CC, it is important to consider HCC–CC if both markers are overlapping or if the antigens corresponding to one tumor are elevated in discordance. Polyclonal CEA when present with cytoplasmic hepatocyte paraffin 1 is sufficient for the diagnosis of HCC. CC in cirrhotic livers is difficult to diagnose and may be mistaken for HCC, which further reinforces the importance of utilizing serum tumor markers and atypical vascular enhancement patterns along with core needle biopsies to reach a proper diagnosis (Figs. 1, 2, 3).

Composite hepatocellular carcinoma and cholangiocarcinoma

Classic discriminating features such as biliary duct dilation and characteristic enhancement patterns may not always be present [9]. The degree of attenuation, signal intensity, and specific enhancement patterns relate to the proportional dominance and distribution of the HCC and CC component within the composite tumor [30]. Dynamic contrast-enhanced MRI and CT are the imaging modalities of choice [31]. HCC characteristically display arterial hyperenhancement with washout during the portal venous or delayed phase and a hallmark enhancing pseudocapsule on delayed phase images [31]. HCC is also strongly associated with vascular invasion of the portal or hepatic venous system CCs have varied enhancement patterns but generally display a continuous peripheral rim enhancement during early phase with hyperenhancement in the central portion of the tumor and peripheral washout in the delayed phase [9]. Progressive centripetal enhancement of fibrous stroma, capsular retraction, and associated biliary ductal dilatation should be noted on CT [9]. HCC–CC tumors may demonstrate enhancement patterns of both HCC and CC, with the HCC component showing early enhance-

ment with delayed washout as well as the CC component demonstrating delayed enhancement [32]. MRI may further identify intratumoral lipid and fibrotic patterns for scirrhous HCC [9]. Figure 1 demonstrates a more common case of biphenotypic liver tumor that presents with predominantly CC features but reveals a HCC component upon histological examination.

Aoki et al. present one example of an effort to differentiate HCC–CC into three subtypes based on imaging enhancement patterns alone; Type A: HCC–CC involves early phase peripheral enhancement by the HCC component with central hyperenhancement of the CC component and peripheral washout on the delayed phase; Type B: HCC–CC involves predominantly HCC characteristics with early phase hyperenhancement and diffuse washout on delayed phase; Type C: HCC–CC with a more equivocal presentation with a low density mass without enhancement [33].

Imaging pearl

Composite hepatocellular cholangiocarcinoma should be considered when imaging features overlap between those of HCC (arterial phase hyperenhancement, delayed phase washout/capsule appearance, and tumor thrombus) and cholangiocarcinoma (continuous peripheral arterial hyperenhancement, progressive centripetal enhancement, capsular retraction, and biliary ductal dilatation), or if the AFP and CA19-9 are either both elevated or divergent.

Hepatobiliary collision tumors

Liver collision tumors are generally more common than composite tumors [34, 35]. Typically, focal hepatic lesions in cirrhotic livers should be regarded as suspicious for HCC until proven otherwise. However, the risk of false diagnosis of HCC by contrast MRI should be

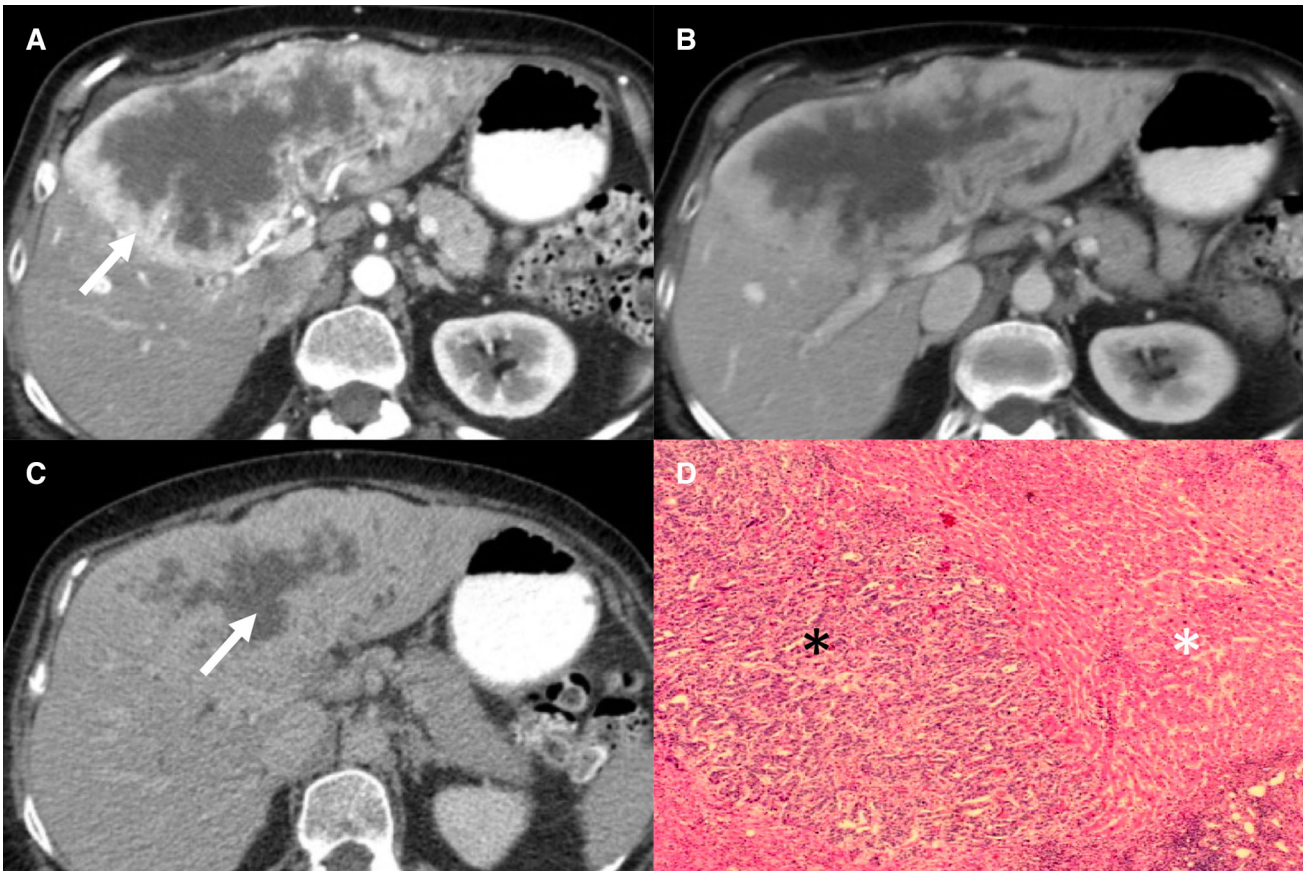

Fig. 1. 68-year-old female with biliary obstruction and initial imaging with liver ultrasound demonstrating a large nonspecific hypoechoic mass in the left hepatic lobe of the liver. Contrast-enhanced arterial (**A**) and venous (**B**) phase CT demonstrates a large heterogeneously enhancing, centrally necrotic mass occupying almost the entire left hepatic lobe with continuous peripheral enhancement characteristic of CC (*black arrow*). Enhanced delayed phase CT (**C**) demonstrates progressive centripetal enhancement (*white arrow*). The imaging features are characteristic of CC, which is frequently the case for composite HCC–CC, requiring tissue sampling to suggest the correct diagnosis. (**D**) H & E stain at ×4 magnification shows an admixture of classic HCC with pseudoglands and hyperchromatic nuclei (*black asterisk*) adjacent to the interhepatic glandular forming CC with a finely granular eosinophilic cytoplasm (*white asterisk*).

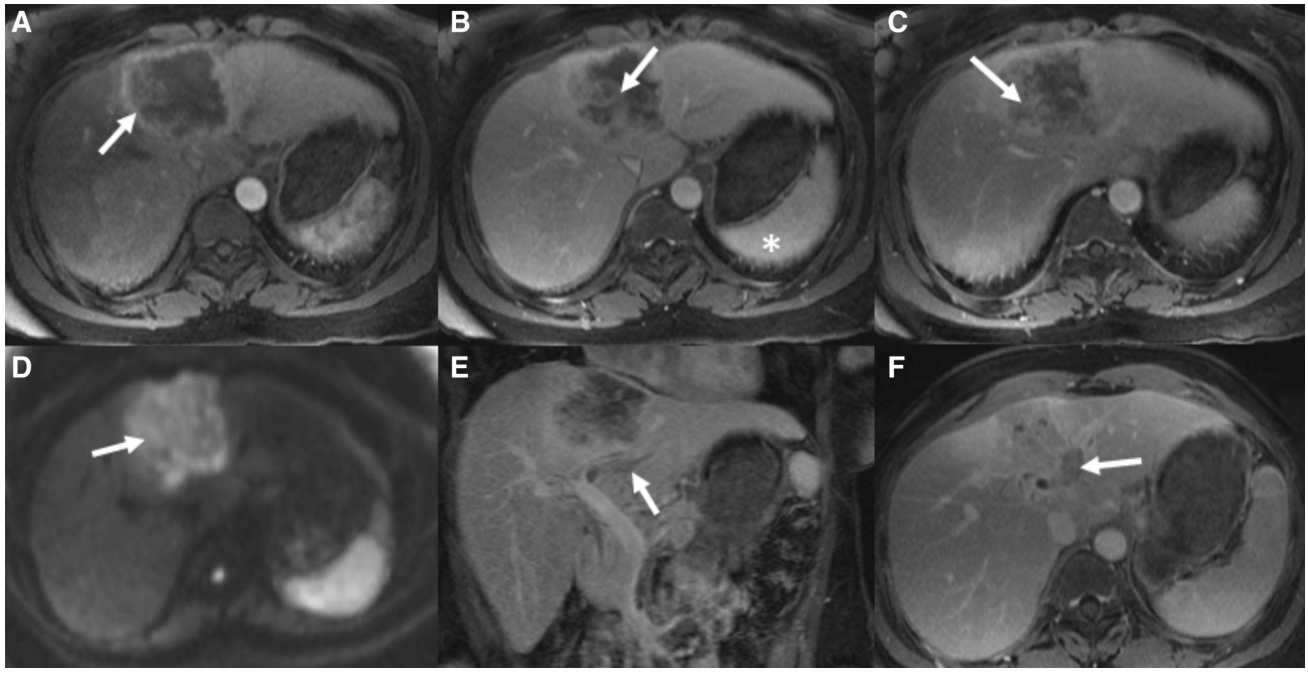

Fig. 2. 53-year-old female with hepatitis C presenting with abdominal pain and weight loss. MR images demonstrate a large segment 4 mass (*white arrow*) with a continuous rim of peripheral arterial enhancement (**A**) and progressive centripetal enhancement on portal venous (**B**) and 5-min delayed images (**C**). The mass demonstrates marked diffusion restriction (**D**). There is associated tumor thrombus (*white arrow*) in the left portal vein (**E** and **F**). The enhancement pattern is characteristic of cholangiocarcinoma, but the presence of vascular invasion and an elevated AFP (>3000 ng/mL) raised suspicion for a composite HCC-cholangiocarcinoma that was confirmed pathologically with immunohistochemical evidence of CK7, CK9, CD10, and polyclonal CEA positivity.

considered in particular cases where CC is also suspected [34–36].

Collision of cholangiocarcinoma and hamartoma

Hepatic mesenchymal hamartoma are considered uncommon benign hepatic tumors or even developmental anomalies rather than a cystic neoplasm [37, 38]. Clinically, children with hepatic mesenchymal hamartomas present with abdominal enlargement and respiratory distress while adults do not have a definitive presentation. Hamartomatous lesions are composed of an admixture of hepatic structures ranging from blood vessels and bile ducts to small groups of hepatocytes within edematous connective tissue stroma [39, 40].

On unenhanced CT, hamartomas usually appear heterogeneous with hypoattenuating stromal elements [40, 41]. The alternating solid and cystic components of hamartomas may appear to have a "swiss cheese" like pattern. On post-contrast CT, thick solid septa of the hamartoma may demonstrate heterogeneous enhancement [39, 42–44] Mesenchymal hamartomas in adults may show a series of histologic modifications: progressive loss of hepatocytes, degeneration of bile duct epithelium, and cystic changes of the mesenchymal component. Mesenchymal hamartomas are benign lesions, which typically have the best prognosis when treated with surgical resection due to potential growth/-mass effect and risk of malignant degeneration [45]. Ultrasound-guided intraoperative aspiration of fluid from cystic components of the hamartomas to reduce its volume may facilitate surgical resection [44]. Other possible differential diagnoses for hepatic lesions including hepatic abscess, hepatic embryonal sarcoma, infantile hemangioendothelioma of liver, simple cysts, hemorrhagic cysts, and hepatoblastoma should be considered and correlated with the patient's clinical presentation and medical history (Fig. 4).

Collision tumor with focal nodular hyperplasia and carcinoma

Figure 5 presents the collision between focal nodular hyperplasia and poorly differentiated carcinoma of the liver. Focal nodular hyperplasia is considered the second most prevalent benign tumor of the liver after hepatic hemangioma, and is typically associated with no malignant potential.

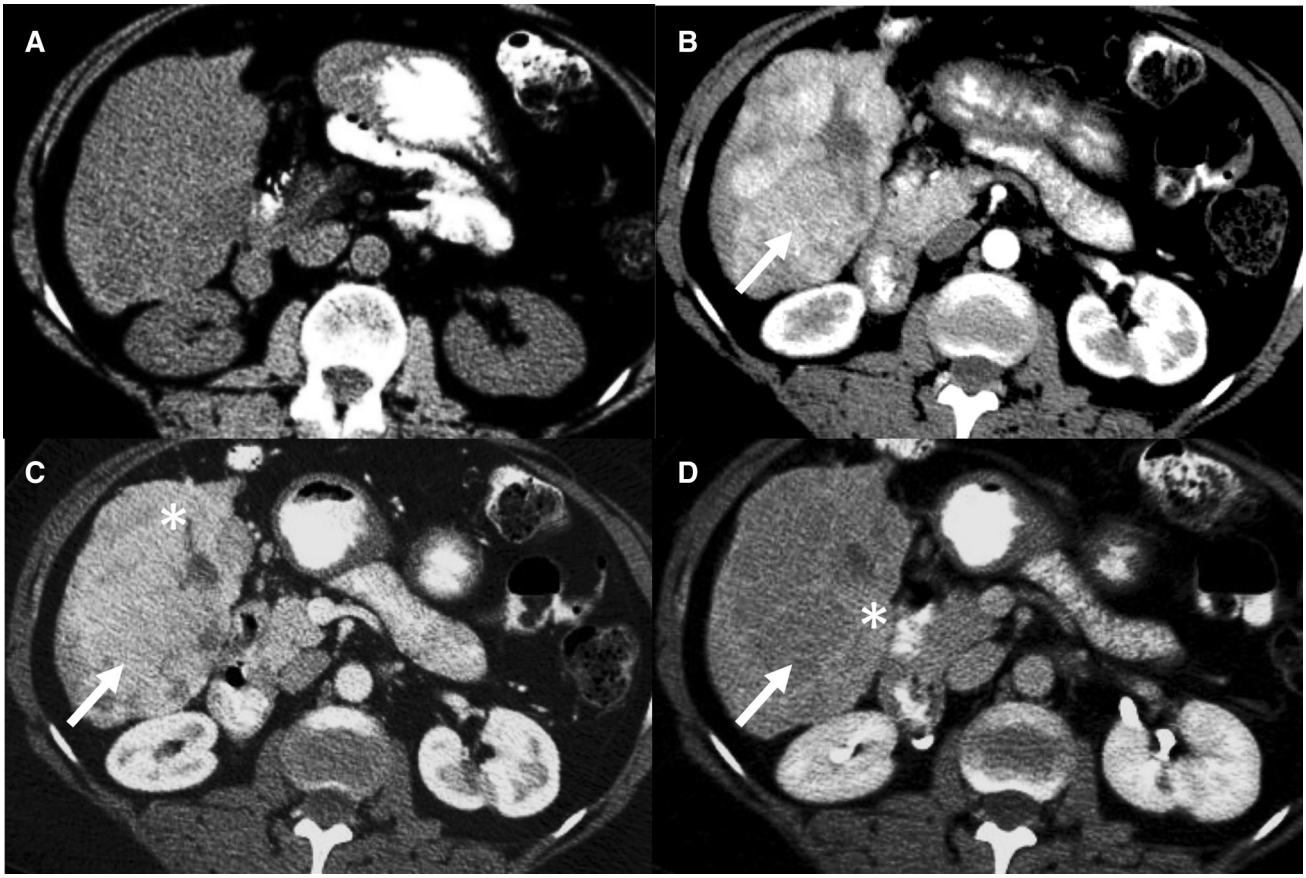

Fig. 3. 57-year-old male with elevated AFP of 140,000 and moderately elevated CA19-9. Noncontrast CT (**A**) shows heterogenous low to isoattenuation mass in segment VI of the liver. On arterial (**B**), portal venous (**C**), and delayed phase (**D**) contrast-enhanced CT images, the mass shows a distinct delayed enhancing component which was pathologically cholangiocarcinoma (*white asterisk*) and a briskly enhancing component with definite washout representing the HCC component (*white arrows*).

Imaging pearl

Hepatic collision tumors should be suspected when a liver lesion has distinct morphologic components, but no pathognomonic features are available to confirm this rare diagnosis without tissue sampling.

Genitourinary composite tumors

True composite renal tumors are rare findings and should be differentiated from the more common scenario of two synchronously occurring renal tumors in close proximity with lack of cellular admixing [46]. Renal cell carcinomas (RCCs) are malignant neoplasms that arise from tubular epithelium. RCCs in general constitute 90% of all renal neoplasms, of which the clear cell RCC subtype is most common (70%–75% of all RCC cases) with the poorest overall prognosis, while chromophobes and papillary RCC subtypes constitute only 5 and 10%, respectively [47]. Mixed papillary and clear cell RCC tumors are considered the single most commonly occurring renal composite tumor [46]. Although most composite RCC chromophobe and oncocytoma tumors are indolent, a small fraction of these tumors may behave more aggressively [48].

Individuals with hereditary papillary RCC associated with changes in the *MET* gene may have the tendency for developing multiple tumors that typically doesn't spread to any other part of the body [49]. Extremely rare subtypes that constitute less than 1% of RCC includes collecting duct RCC, multilocular cystic RCC, medullary carcinoma, neuroblastoma-associated RCC, mucinous tubular, and spindle cell carcinomas. The remaining 5%–10% of renal cancers includes transitional cell carcinoma of the renal collecting system [50]. Renal sarcomas that manifest in blood vessels or connective tissue and unclassified renal cell carcinomas constitute less than 1% of all renal cancers. Benign renal tumors include renal adenoma, oncocytoma, and angiomyolipoma. Identifying the presence of a composite tumor on imaging and its subtypes has significant prognostic and therapeutic implications for surgical planning and resection, and also for inoperable patients for whom radiation, immunotherapy, and molecular-targeted therapy may be more appropriate [51, 52].

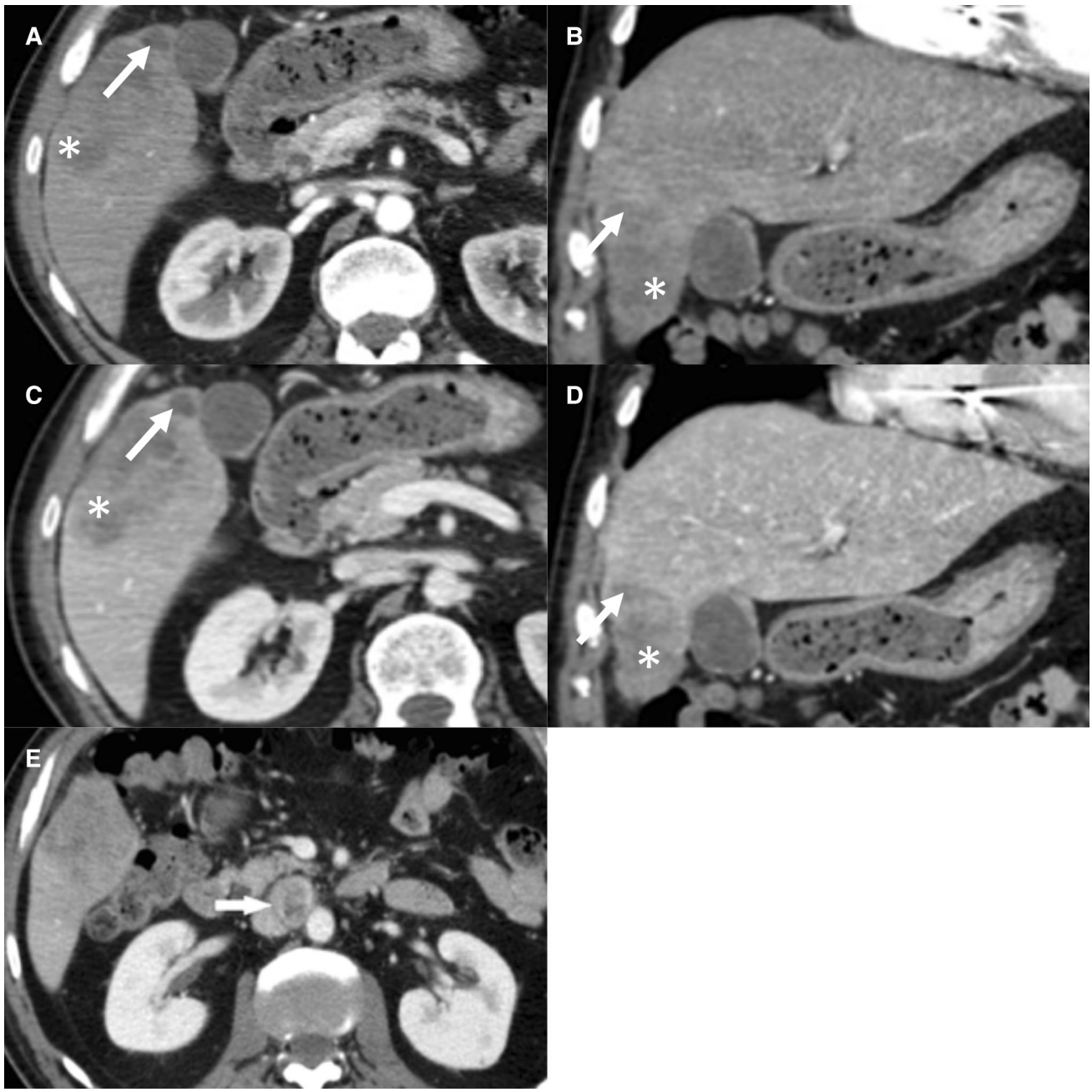

Fig. 4. 69-year-old male with a liver of normal contour and size presents with abdominal pain. Axial (**A**) and coronal (**B**) post-contrast CT arterial and axial phase (**C**) and coronal (**D**) portal venous phase demonstrates a predominantly hypoattenuating mass (suggesting central areas of necrosis) with rim enhancement within segment 5/6 of the liver concerning for primary hepatic neoplasm or metastatic lesion. Pathology demonstrated the presence of cholangiocarcinoma (*white arrow*) and hamartoma (*white asterisk*). Aortocaval lymphadenopathy at the level of the kidney (*broad white arrow*) is highly suspicious for nodal metastasis (**E**).

Composite papillary and clear cell renal cell carcinoma

Mixed papillary and clear cell RCCs composite tumor involves the histologic comingling of each individual subtype leading to an image appearance atypical for either disease entity [46]. Clear cell RCC recapitulates the epithelium of the proximal convoluted tubules, and are composed of cells with abundant optically clear cell cytoplasm visible on histology [53]. 95% of clear cell RCCs are sporadic and associated with 3p deletions that involve somatic inactivating mutations of the von Hippel Lindau gene [54].

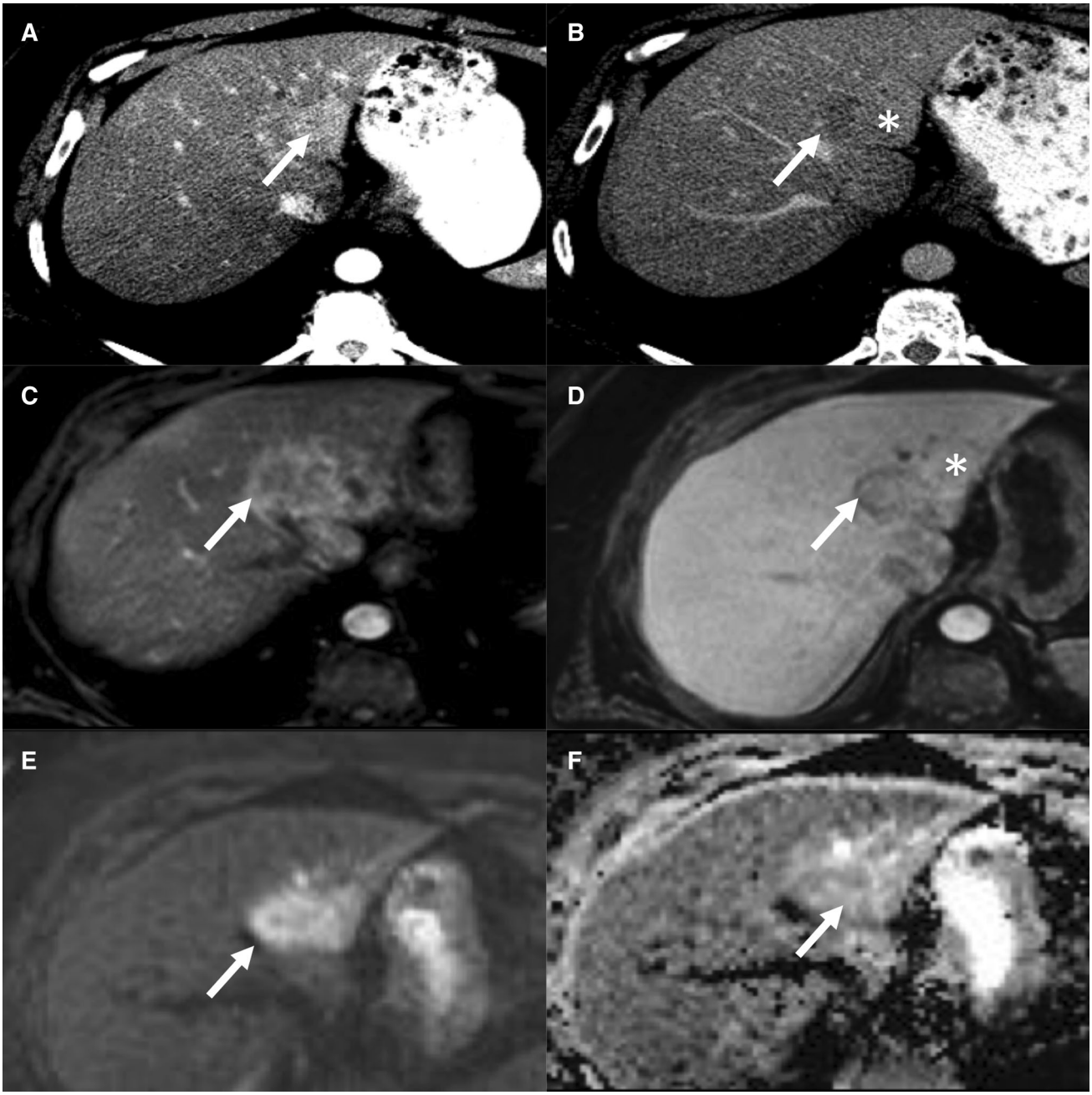

Fig. 5. 62-year-old female with history of clear cell bladder cancer, melanoma, and basal cell carcinoma presenting with collision of focal nodular hyperplasia and poorly differentiated carcinoma. Multiphasic CT shows a 3 cm left lobe liver lesion showing brisk enhancement (*white arrow*) on the arterial phase enhancement (**A**), with 3 min delayed washout (**B**) laterally (*white arrow*) and contrast retention medially (*white asterisk*). Biopsy of the medial (*white asterisk*) area demonstrated FNH and steatohepatitis while biopsy of the lateral area (*white arrow*) revealed poorly differentiated carcinoma. MRI of the abdomen demonstrates an arterially enhancing mass (**C**, *white arrow*). 3 min delayed images (**D**) show washout laterally (*white arrow*) and contrast retention medially (*white asterisk*). Diffusion-weighted imaging (**E**) demonstrates restricted diffusion of the lateral component confirmed by ADC map (**F**) (*white arrows*).

Composite papillary and clear cell carcinomas typically present with mixed imaging patterns and vascular enhancement patterns atypical for papillary RCC. Papillary RCCs are typically small neoplasms that characteristically appear hypointense on T2-weighted images due to the presence of hemosiderin deposition, hemorrhage, or necrosis, and often have a fibrous capsule [55]. MRI of composite papillary and clear cell RCC has been previously reported to present with an atypical brisk nodular enhancement at the periphery of the lesion [46]. Clear cell RCC presents as a cortically based mass with signal intensities similar to that of renal parenchyma on

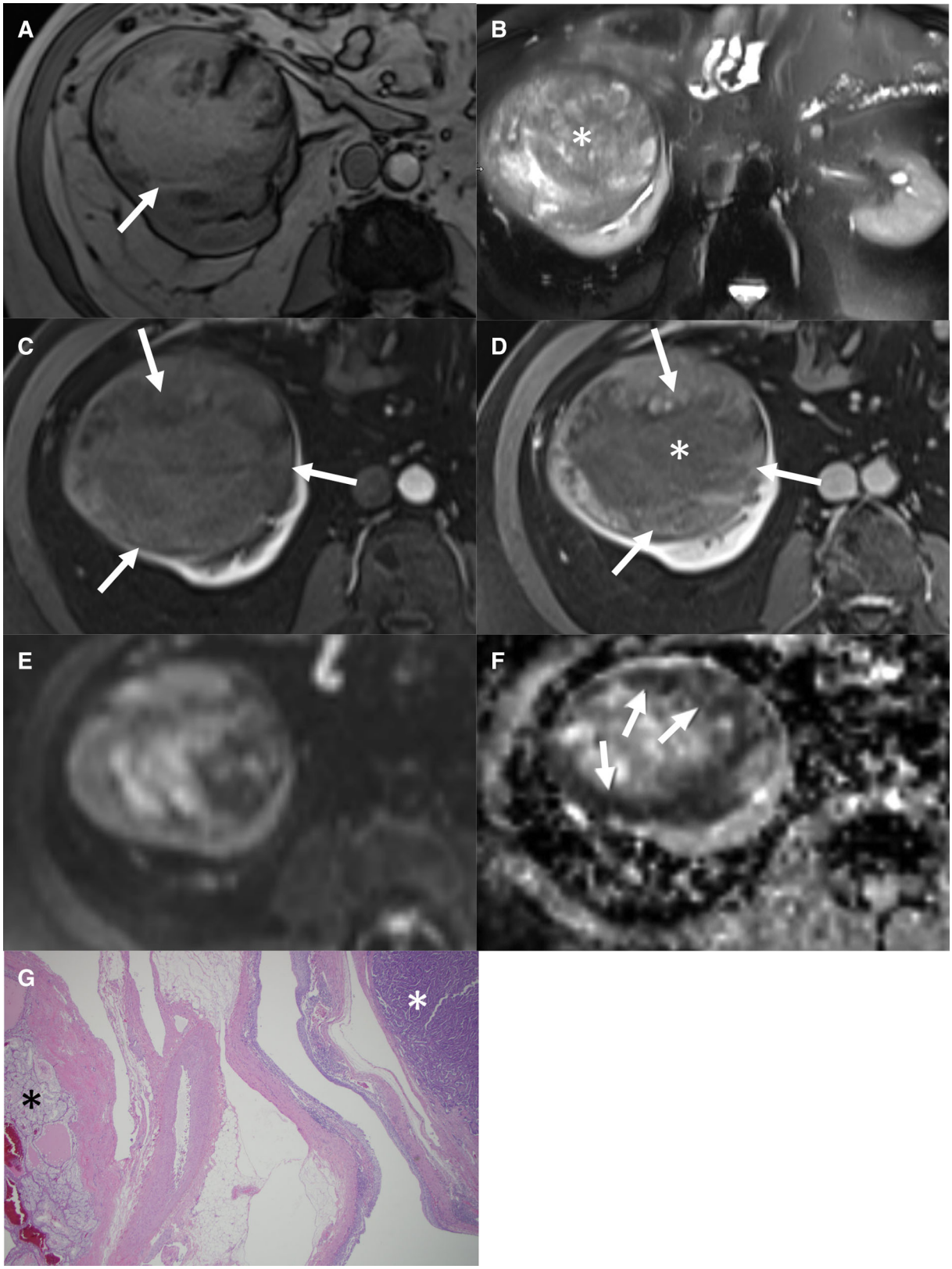
A
B
C
D
E
F
G

◀**Fig. 6.** 62-year-old male presenting with right flank pain and hematuria. Out-of-Phase T1-weighted MRI (**A**) demonstrate a large renal mass with heterogeneous intermediate T1 signal. Fat-suppressed T2-weighted MRI (**B**) indicates mainly hypointense T2 signal suggestive of a papillary RCC component (*white asterisk*). Post-contrast arterial phase (**B**) and delayed phase (**C**) MRI demonstrates progressive nodular peripheral enhancement (*white arrows*) characteristic of clear cell RCC, and relative little central enhancement (*asterisk*) consistent with papillary RCC. Restricted diffusion of the peripheral nodular clear cell RCC component (*arrows*) is confirmed by high B value diffusion weight image sequence (**E**) and ADC map (**F**) (*white arrows*). Low power hematoxylin-eosin photomicrograph (**G**) of clear cell renal cell carcinoma (*black asterisk*) with intervening adipose tissue showing a second tumor (*white asterisk*) with features consistent with papillary renal cell carcinoma (type 1).

T1-weighted images and hyperintensity on T2-weighted images, with signal variability attributable to hemorrhage, cystic change, and necrosis [55]. Acknowledging that clear cell RCCs are typically hypervascular, the degree of contrast enhancement during the arterial phase can help identify the difference between clear and non-clear cell subtypes [56]. The greater extent of signal intensity change on the corticomedullary phase sequence is the most specific and sensitive parameter for differentiating clear cell from papillary RCCs [57] (Fig. 6).

Composite papillary renal cell carcinoma and oncocytoma

Oncocytomas are benign kidney tumors typically observed in men with a peak incidence in the seventh decade of life [58]. Oncocytomas although may grow quite large do not typically spread to other organs and is curative by surgical resection. However, differentiating renal oncocytomas from RCC by imaging has proven difficult due to their similar imaging features, requiring pathology to make a confident diagnosis [48]. Results from a meta-analysis across 1711 participants and 21 studies have indicated that expression of CK7 is a major immunohistochemical marker for differentiating RCC from oncocytoma [48]. Oncocytomas enhance avidly and relatively homogeneously during the corticomedullary phase without signs of necrosis or hemorrhage, and may have a low attenuating central stellate scar on CT [59–62]. On MRI, oncocytomas are typically round well-defined masses with hypointense T1 signal and hyperintense T2 signal relative to renal cortex [63] (Fig. 7).

Composite clear cell and chromophobe renal cell carcinoma

Chromophobe is the third most common RCC subtype that appears equally among men and women primarily in the sixth decade, and has the best relative prognosis

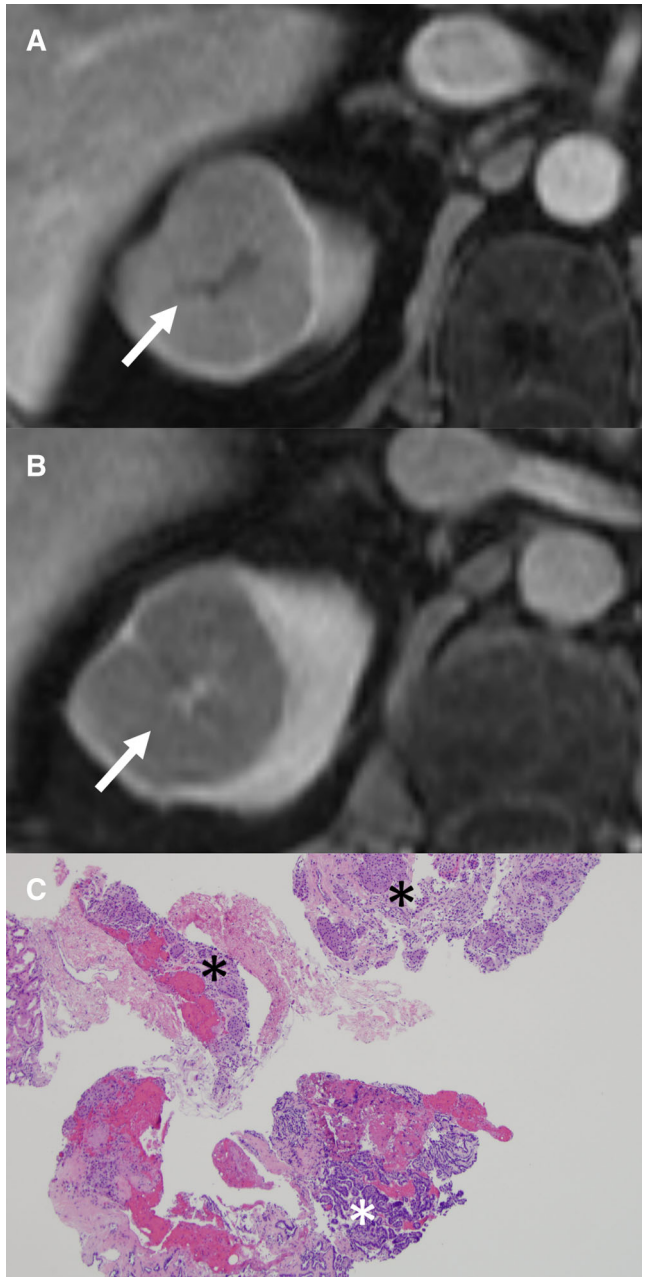

Fig. 7. Asymptomatic 57-year-old man discovered to have a hyperechoic renal mass on sonographic imaging. T1-weighted post-contrast venous phase MRI (**A**) demonstrates a central stellate hypoenhancing scar (*white arrow*). T1-weighted post-contrast delayed phase MRI (**B**) demonstrates a "spoke wheel like" appearance (*white arrow*) suggestive of oncocytoma. Low power hematoxylin-eosin photomicrograph of the surgical tumor (**C**) image reveals classic renal oncocytoma in the upper fragment (*black asterisk*) and papillary renal cell carcinoma in the lower fragment (*white asterisk*). Composite tumors on imaging may sometimes mimic the appearance of a single neoplasm.

amongst the RCC subtypes [64]. Chromophobe RCC appears microscopically as round to polygonal-shaped cells with well-defined cytoplasmic borders, pale to eo-

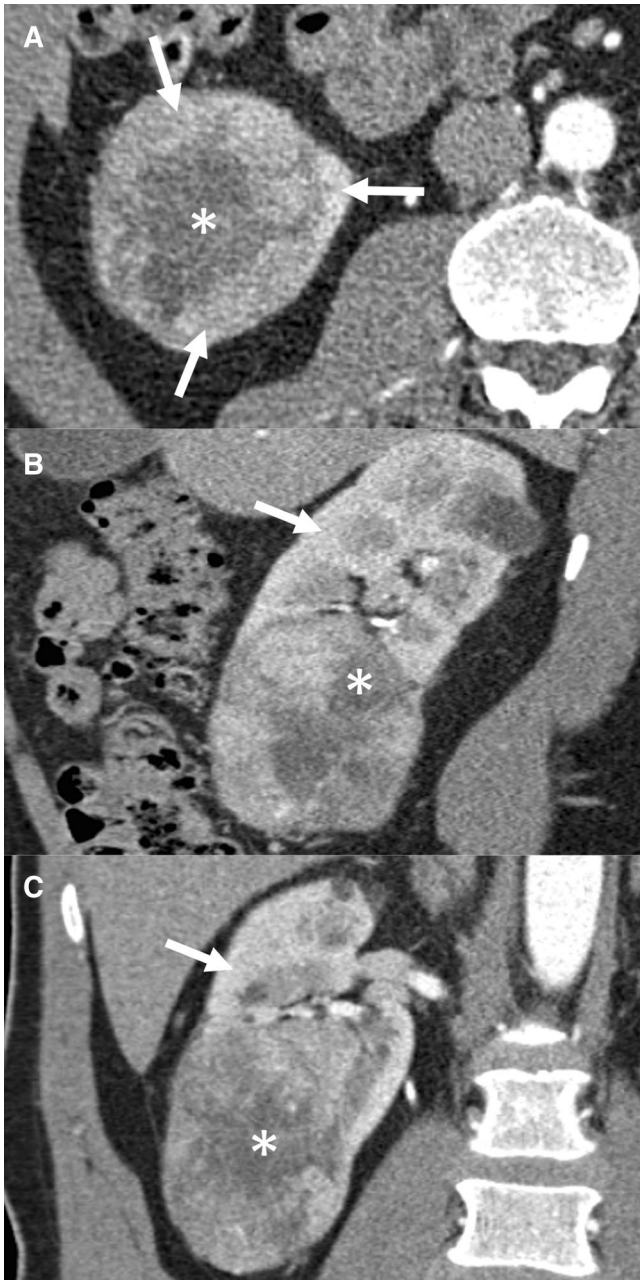

Fig. 8. 54-year-old male presenting with painless hematuria. Coronal (**A**), Axial (**B**), and Sagittal (**C**) post-contrast CT images demonstrates a poorly defined heterogeneous lesion in the inferior pole of the right kidney infiltrating into the interpolar region. Briskly enhancing periphery is characteristic of clear cell RCC (*white arrow*) while the less enhancing central area is a characteristic of chromophobe type RCC, but could also represent necrosis (*white asterisk*). Histopathology confirms a composite tumor composed of a clear cell and chromophobe RCC.

sinophilic cytoplasm, and perinuclear halos on histology [65]. While chromophobe tumor image features include hyperechogenicity on ultrasonography, homogenous enhancement on CT and MRI, and T2 hypointensity on MRI, these imaging features overlap with those of oncocytomas, which are generally indistinguishable from other RCC subtypes [66]. Kondo et al. have reported that although the CT and MRI findings of chromophobe RCC are not uniform, a spoke wheel-like enhancement with a central stellate scar is a hallmark imaging pattern that should be considered for malignancy, but these features similarly overlap with oncocytomas [67]. Chromophobe components on MRI may appear hypointense relative to renal parenchyma on T2-weighted images [55]. In composite clear cell and chromophobe RCCs, clear cell RCC is associated with a much higher degree of enhancement than the chromophobe subtype component (Fig. 8).

Composite clear cell renal cell carcinoma with sarcomatoid focus

Sarcomatoid cells are considered the rarest type of mesotheliomas and are much more aggressive than conventional RCC subtypes [68]. Sarcomatoid renal cell carcinoma is recognized as a transformation of any RCC subtype into a higher histological grade, which is typically characterized by a spindle cell-shaped morphology but demonstrates both epithelial and mesenchymal differentiation on immunohistochemistry [69–71]. Systemic therapy following surgery is the preferred modality of treatment for managing patients with sarcomatoid RCC [68]. Sarcomatoid RCCs are typically associated with larger tumor size, greater peritumoral neovascularity, larger peritumoral vessels, and greater heterogeneity by textural analysis than clear cell RCCs [72] (Figs. 9, 10).

Composite chromophobe and sarcomatoid renal cell carcinoma

Imaging pearl

Composite renal tumors should be suspected when internal components of a renal mass demonstrate unique imaging characteristics such as T2 signal intensity, diffusion restriction, or enhancement pattern that cannot be readily explained by the presence of cystic components or necrosis.

Genitourinary collision tumors

Renal collision tumors refer to a single tumor mass composed of two distinct synchronous primary neoplasms or a combination of a primary and metastatic lesion occurring by coincidence in the same anatomical location within the kidney [46]. In terms of frequency, the collision of simple and or complicated cystic lesions within the renal parenchyma is much more common than the collision of solid tumors and cysts, which is also much more common than the collision of two solid renal tumors [49].

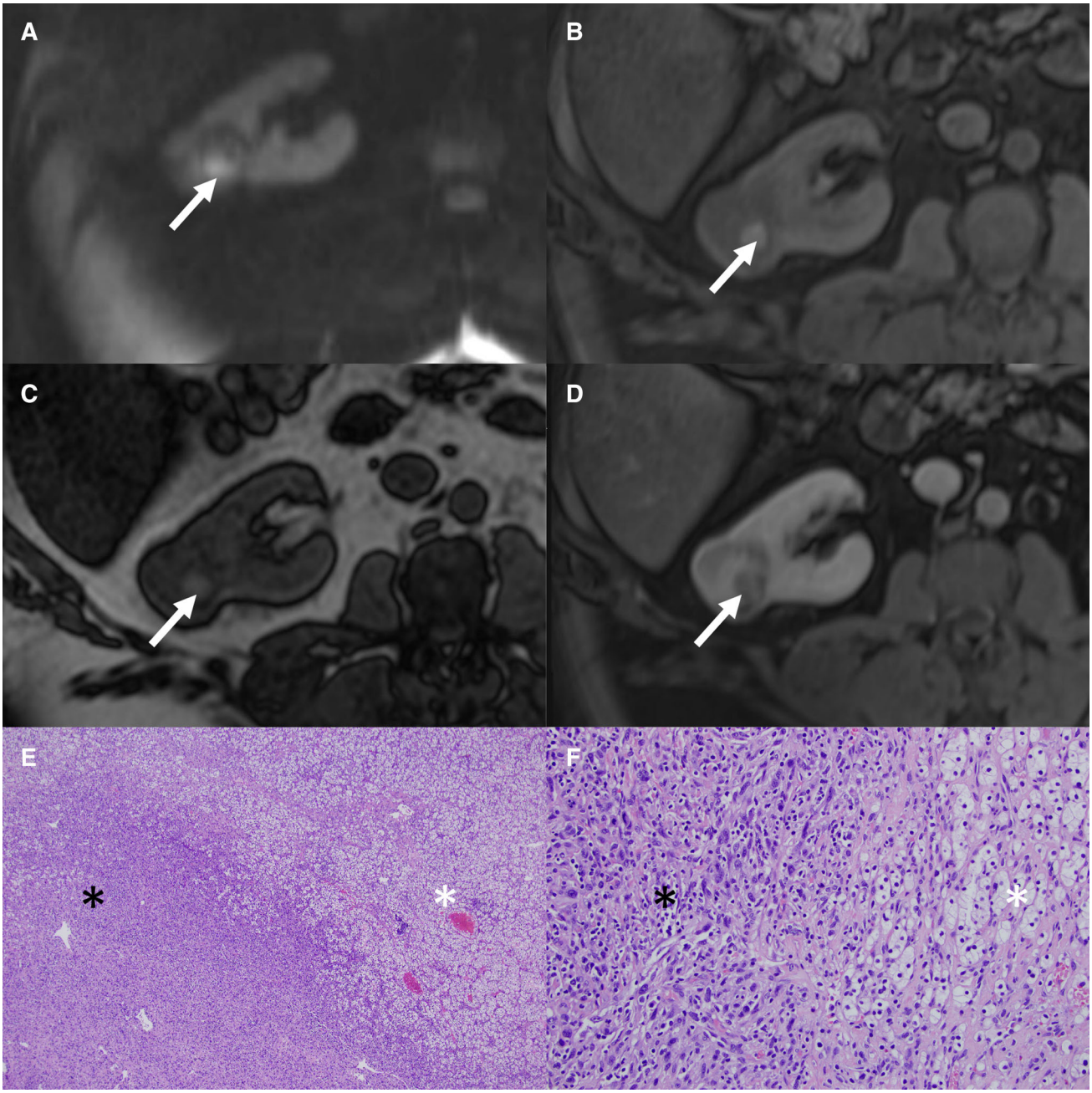

Fig. 9. 57-year-old man with renal mass. Two distinct imaging signatures are noted on MRI. Diffusion-weighted MRI (**A**) demonstrates restricted diffusion within a medial component of the mass (*white arrow*). This same component is also T1 hyperintense on pre-contrast fat-suppressed T1- (**B**) and out-of-phase T1- (**C**) weighted MRI (*arrows*). With contrast administration (**D**), this focus is hypoenhancing (*white arrow*) relative to the surrounding renal mass. H & E stain images at ×4 (**E**) and ×10 (**F**) magnification showing classic spindle cells indicative of sarcomatoid elements on the left of the images (*black asterisks*) and clear cell RCC on the right of the images (*white asterisks*).

Collision renal cell carcinoma and hemorrhagic cyst

Collision of solid and cystic lesions is less frequent than the collision of two simple cysts. ADC and DWI combined with T2-weighted sequences and subtraction imaging are helpful for differentiating RCC from hemorrhagic cysts (Fig. 11).

Collision angiomyolipoma and clear cell renal cell carcinoma

Angiomyolipoma (AML) is the most common benign tumor of the kidney. It is crucial to differentiate AMLs from RCCs as management vastly differs. AMLs may occur simultaneously or adjacent to existing RCC malignant lesions [46]. Biopsy of the AML component

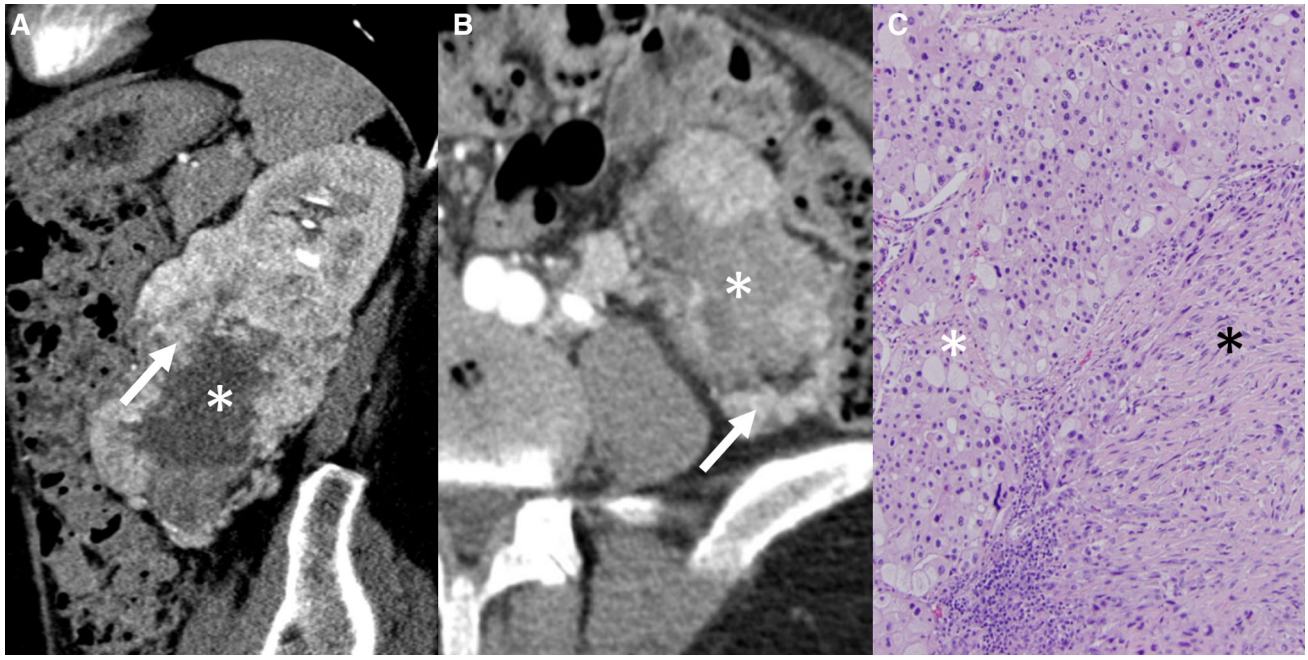

Fig. 10. 67-year-old man with large heterogeneously enhancing left renal mass. Post-contrast sagittal (**A**) and axial (**B**) CT images demonstrate peripheral enhancement of the renal mass (*arrows*) and central hypoattenuation (*asterisks*) likely representing necrosis. Histology (**C**) shows chromophobe cells on the left of slide consistent with chromophobe RCC (*white asterisk*) and classic spindle cells on the right consistent with sarcomatoid elements (*black asterisk*).

typically show muscle and adipose tissue and the RCC will show classic clear polygonal cells, which have an eosinophilic cytoplasm, atypical nucleus, and inconspicuous nucleoli. Figure 12 demonstrates the rich vascularization associated with the benign AML may actually enhance the growth of the nearby RCC in select cases of AML-RCC. AML components can typically be identified and differentiated from RCCs by the presence of bulk fat on CT and MRI. However, studies have demonstrated that 4.5% of AMLs with atypical abnormal muscle and blood vessel predominance may have minimal fat composition, complicating a straightforward imaging diagnosis [73].

Imaging pearl

Renal collision tumors are more common than composite tumors and can be suggested by the presence of fat or hemorrhagic components in one of the two moieties to distinguish it from the other component.

Adrenal collision tumors

Many adrenal collision tumors go undetected due to their small size. The most common tumors of the adrenal gland include adenoma, metastases, pheochromocytoma, and adrenocortical carcinoma. The prevalence of adrenal adenoma is correlated with age, where Kloos et al. reported patients from 20 to 29 years of age have a frequency of 14% for discovering unsuspected adenoma compared to 7% in populations over 70 years of age using CT [74]. Although most adrenal incidentalomas are asymptomatic and coincidentally detected on imaging, exceptions including adrenocortical carcinomas and pheochromocytomas that require therapeutic intervention.

Multi-detector CT, MRI, and PET/CT are each valuable for detecting and diagnosing adrenal collision tumors. Attenuation values for conventional and enhanced CT imaging and washout characteristics for delayed images can be leveraged to differentiate benign and malignant components for adrenal cortical tumors. MRI with chemical shift imaging and gadolinium-enhanced techniques are indicated when there are equivocal findings on CT [75]. Adenomas have well demarcated borders and homogenous central signal [76]. Hemorrhage within adenomas or any type of fibrosis and fatty metaplasia within an adrenal neoplasm may mimic an adrenal collision tumor [75]. PET/CT may be helpful in selective cases of functional malignant masses where there is the presence of contralateral adrenal atrophy. The majority of adrenal lesions detected at CT are benign [77]. Other less common adrenal lesions to be aware of when considering an adrenal collision tumor include cystic lesions such as adrenal epithelial cysts, hydatid, and endothelial cysts as well as solid lesions such as angiosarcoma, ganglioneuroma, hemangioma, primary malignant melanoma, and also myelolipomas [78].

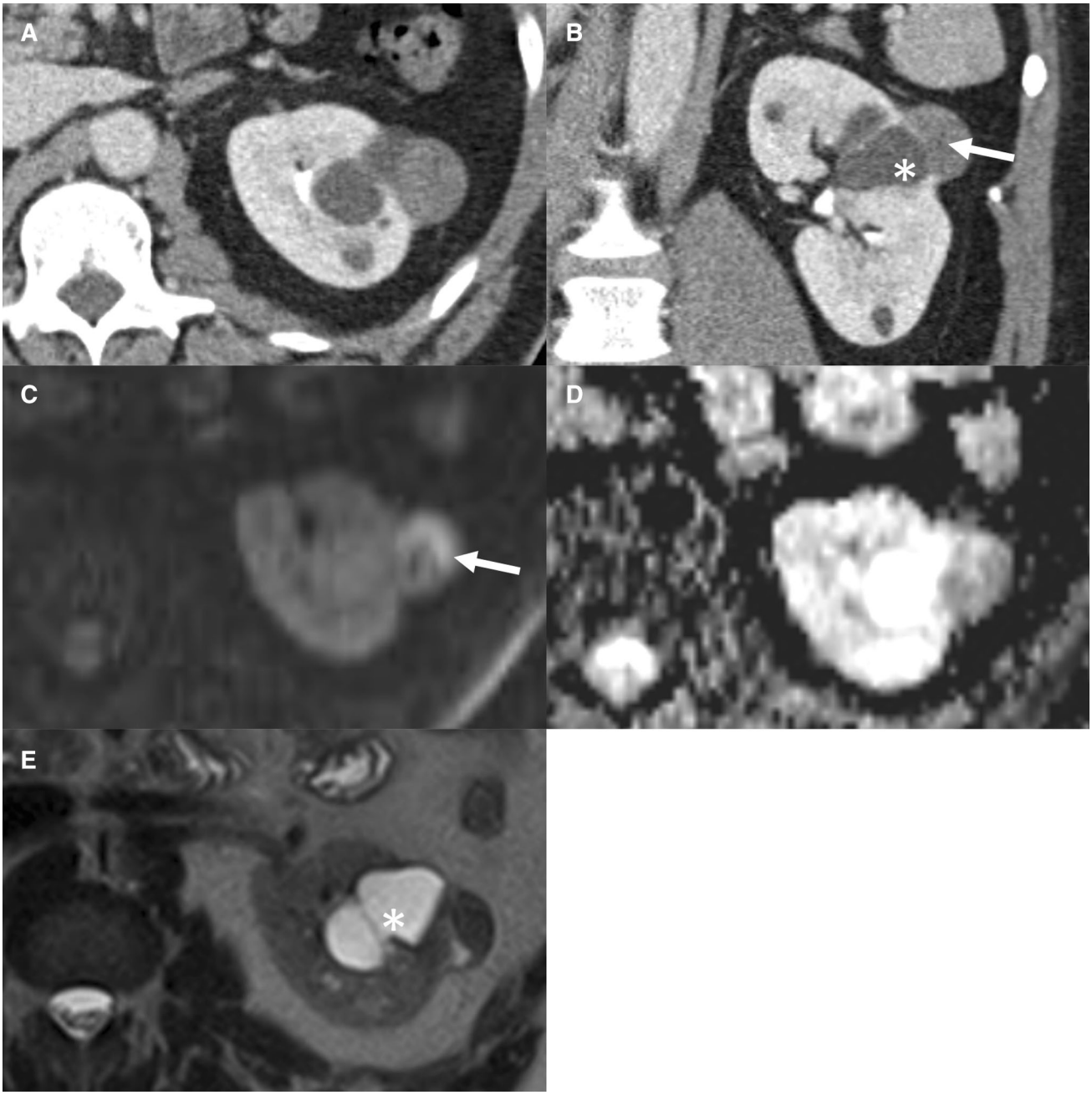

Fig. 11. 50-year-old male presenting for follow-up imaging after discovery of a complex cyst. Post-contrast axial (**A**) and coronal (**B**) CT images reveal a hyperattenuating exophytic lesion in the left kidney (*arrow*) adjacent to a simple cyst (*asterisk*). Diffusion-weighted MRI (**C**) and ADC map (**D**) indicates the presence of cellularity within the lateral component (*white arrow*) colliding with a simple cyst (*white asterisk*), which is hyperintense (*asterisk*) on T2-weighted imaging (**E**). Histopathology confirmed the presence of a malignant neoplasm colliding with a renal cyst.

Collision of pheochromocytoma and adrenal adenoma

The diagnosis of pheochromocytoma includes biochemical analysis of catecholamine levels, particularly metanephrines due to its high sensitivity, prior to biopsy or resection to ensure that alpha-adrenergic blockade can be achieved to avoid potentially devastating procedural complications. Adrenal adenomas have varying quantities of cytoplasmic fat and have heterogeneous appearance while pheochromocytomas have high signal intensities with a ''light bulb sign'' on T2-weighted images [75]. Attenuation values of 10 HU or less on CTis diagnostic for adrenal adenoma [79].

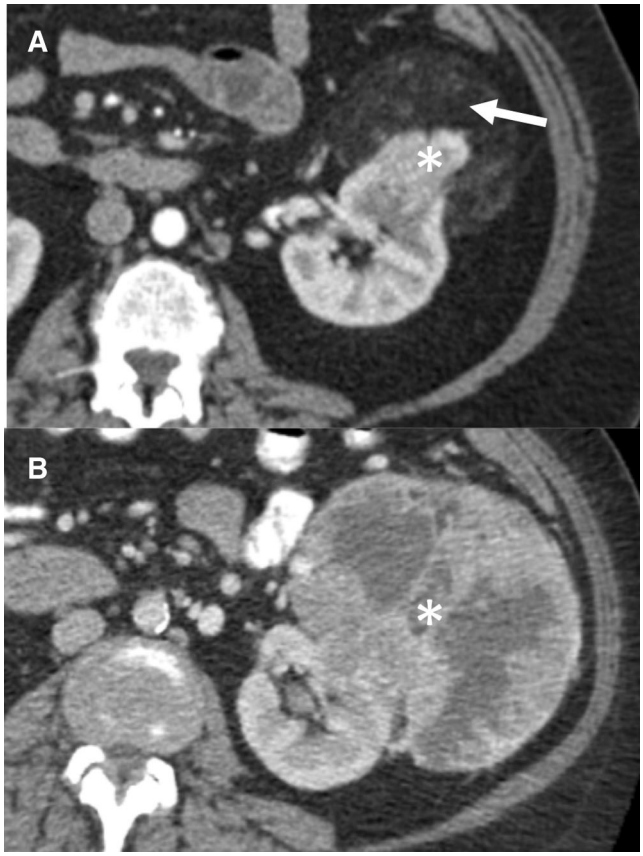

Fig. 12. A 62-year-old man present with subsequent surveillance CT 2 years after initial interpretation. Arterial phase axial CT (**A**) demonstrates a fat-containing mass compatible with AML (*white arrow*). However, there is enhancement of the medial component of the mass (*white asterisk*), with a more inferiorly positioned, delayed image (**B**) demonstrating a bulky, heterogenous mass (*asterisk*) consistent with clear cell RCC colliding with an AML, confirmed pathologically.

Metaiodobenzylguanidine (MIBG) scintigraphy or PET/CT may be employed in cases where CT and MRI are equivocal or there is a high degree of suspicion for an imaging occult pheochromocytoma (Fig. 13).

Collision of primary adrenal adenoma and metastatic renal cell carcinoma

This case reflects the hypothesis that the first tumor may have altered the microenvironment within the organ in such a way that it will more likely be facilitate metastatic seeding. Incidental adrenal lesions are common in patients with primary RCC, which may be difficult to differentiate from adrenal adenomas due to signal dropout on chemical shift MRI [80]. Most adrenal adenomas are nonfunctional; however, the presence of contralateral adrenal atrophy may suggest otherwise [81]. On CT imaging, adrenal adenomas are typically well-defined homogeneous lesions that range up to 2.5 cm [82] (Fig. 14).

Imaging pearl

Adrenal collision tumors can be overlooked or misdiagnosed if all components of the entire adrenal mass are not carefully evaluated. This has greater relevance in detecting a potentially malignant component within a lesion that might otherwise be characterized as benign, than vice versa.

Conclusion

The spectrum of hepatic, renal, and adrenal composite and collision tumors have been reviewed in these illustrative cases. Composite tumors have a common cellular origin with intermingling of cells in histology while collision lesions are histologic distinct but adjacent lesions in the same organ. The presence of two different cell types can sometimes lead to perplexing imaging findings, which at times can make an imaging diagnosis challenging and may necessitate biopsy (of both components) for confirmation. Although rare, it is important to clinically recognize these tumors since biopsy of only the benign component can have adverse consequences. The appearance of collision and composite tumors is atypical for any single histopathologic tumor type, but rather an exceptional imaging appearance, at times combining characteristics of both tumors.

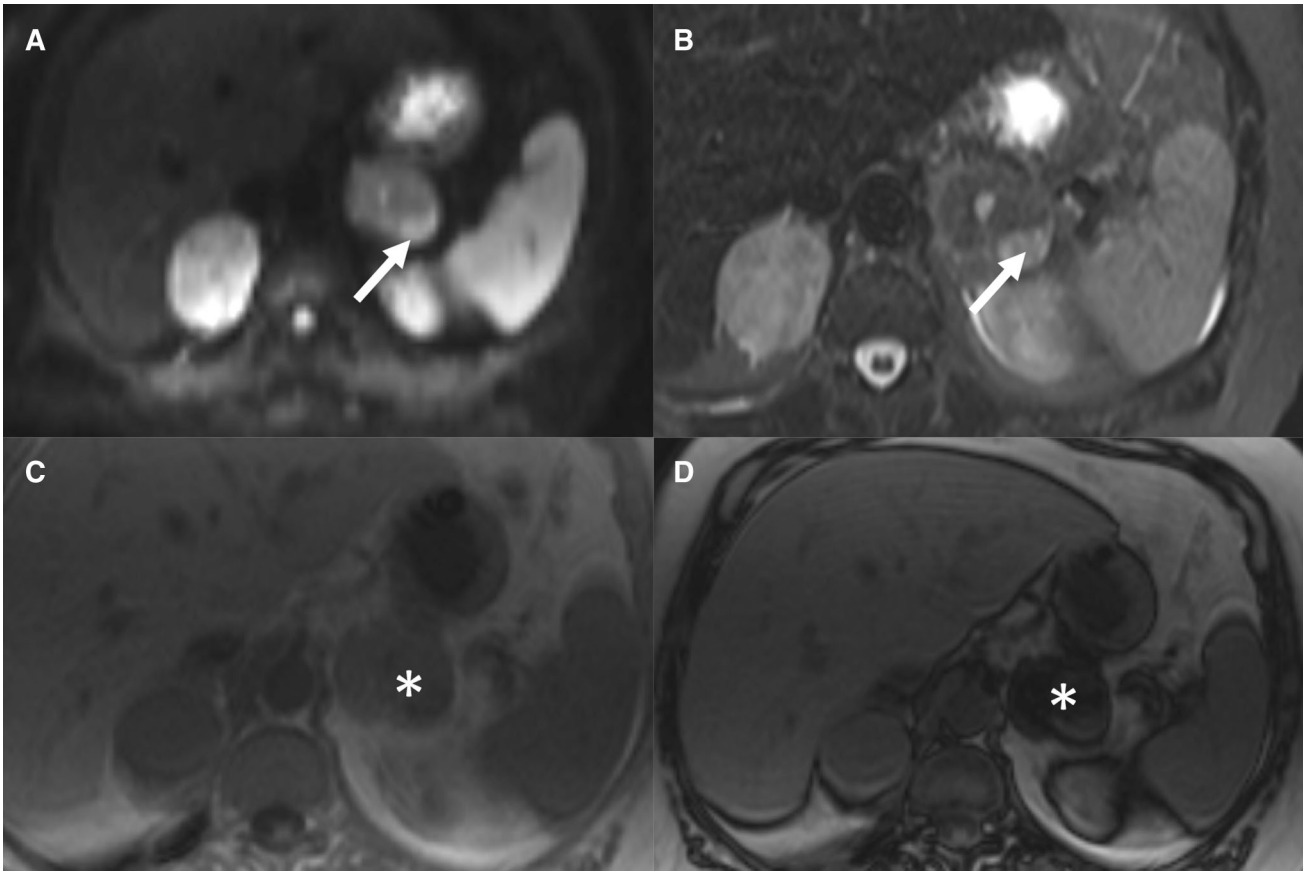

Fig. 13. 72-year-old woman presenting in hypertensive crisis found to have markedly elevated urine metanephrines and free catecholamines. The lateral component of the well circumscribed mass (*white arrow*) shows marked diffusion restriction (**A**) and appears T2 hyperintense (**B**), in keeping with pheochromocytoma (*white arrow*). T1-weighted in-phase (**C**) and out-of-phase (**D**) sequences demonstrate signal loss in the larger, medial component of the mass, consistent with adenoma (*white asterisk*), without signal loss in the lateral pheochromocytoma component. Histopathology confirmed the pheochromocytoma and presence of an adrenal adenoma.

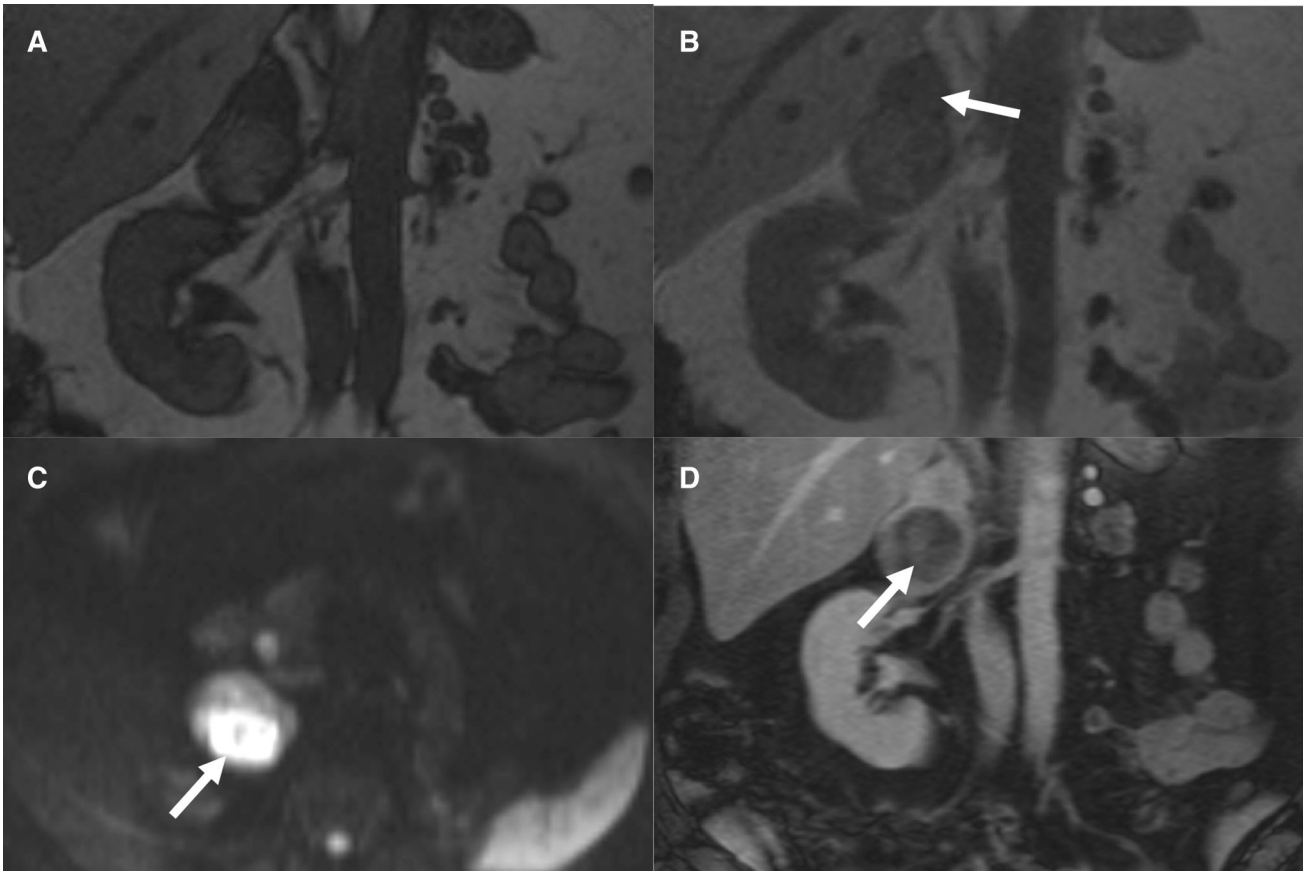

Fig. 14. A 72-year-old woman presents in hypertensive crisis, and is found to have markedly elevated urine metanephrines and free catecholamines. T1-weighted opposed-phase (**A**) and in-phase (**B**) MRI demonstrate signal loss (*white arrows*) within the more superior component of the bi-lobed right adrenal mass, consistent with an adrenal adenoma. Diffusion-weighted MRI demonstrates restricted diffusion in the larger inferior component (**C**, *white arrow*) and peripheral enhancement with central necrosis on coronal T1-weighted post-contrast MRI (**D**, *white arrow*), consistent with metastatic renal cell carcinoma that was confirmed by histopathology.

Compliance with ethical standards

Funding No funding was received for this study.

Conflict of interest The authors declare that they have no conflict of interest.

Ethical approval For this type of study formal consent is not required.

Informed consent Informed consent was obtained from all individual participants included in the study.

References

1. Otal P, et al. (1999) *Imaging Features of Uncommon Adrenal Masses with Histopathologic Correlation1*. http://dx.doi.org/10.1148/radiographics.19.3.g99ma07569.
2. Nayyar M, et al. (2014) Composite liver tumors: a radiologic-pathologic correlation. Clin Mol Hepatol 20(4):406–410
3. Michalinos A, Constantinidou A, Kontos M (2015) Gastric collision tumors: an insight into their origin and clinical significance. Gastroenterol Res Pract 2015:314158
4. Aggarwal N, et al. (2012) Tumor-to-tumor metastasis: case report of a pulmonary adenocarcinoma metastatic to a clear cell renal cell carcinoma. Pathol Res Pract 208(1):50–52
5. Anani W, et al. (2014) A series of collision tumors in the genitourinary tract with a review of the literature. Pathol Res Pract 210(4):217–223
6. Yao B, et al. (2015) A collision tumor of esophagus. Int J Clin Exp Pathol 8(11):15143–15146
7. Brandwein-Gensler M, Urken M, Wang B (2004) Collision tumor of the thyroid: a case report of metastatic liposarcoma plus papillary thyroid carcinoma. Head Neck 26(7):637–641
8. Chin S, Kim Z (2014) Sarcomatoid combined hepatocellular-cholangiocarcinoma: a case report and review of literature. Int J Clin Exp Pathol 7(11):8290–8294
9. Shetty AS, et al. (2014) Combined hepatocellular-cholangiocarcinoma: what the radiologist needs to know about biphenotypic liver carcinoma. Abdom Imaging 39(2):310–322
10. Jarnagin WR, et al. (2002) Combined hepatocellular and cholangiocarcinoma: demographic, clinical, and prognostic factors. Cancer 94(7):2040–2046
11. Lee SD, et al. (2014) Clinicopathological features and prognosis of combined hepatocellular carcinoma and cholangiocarcinoma after surgery. Hepatobiliary Pancreat Dis Int 13(6):594–601
12. Lee JH, et al. (2011) Long-term prognosis of combined hepatocellular and cholangiocarcinoma after curative resection comparison with hepatocellular carcinoma and cholangiocarcinoma. J Clin Gastroenterol 45(1):69–75
13. Yin X, et al. (2012) Combined hepatocellular carcinoma and cholangiocarcinoma: clinical features, treatment modalities, and prognosis. Ann Surg Oncol 19(9):2869–2876

14. Panjala C, et al. (2010) The diagnostic conundrum and liver transplantation outcome for combined hepatocellular-cholangiocarcinoma. Am J Transplant 10(5):1263–1267
15. Liu CL, et al. (2003) Hepatic resection for combined hepatocellular and cholangiocarcinoma. Arch Surg 138(1):86–90
16. Wang J, Wang F, Kessinger A (2010) Outcome of combined hepatocellular and cholangiocarcinoma of the liver. J Oncol 2010:7
17. Chi M, et al. (2012) Management of combined hepatocellular-cholangiocarcinoma: a case report and literature review. Gastrointest Cancer Res 5(6):199–202
18. Sapisochin G, et al. (2011) Mixed hepatocellular cholangiocarcinoma and intrahepatic cholangiocarcinoma in patients undergoing transplantation for hepatocellular carcinoma. Liver Transpl 17(8):934–942
19. Theise N, et al. (2010) Combined hepatocellular-cholangiocarcinoma. In: Bosman FT, Carneiro F, Hruban RH, Theise ND (eds) *Who classification of tumours of the digestive system*. Lyon: International Agency for Research on Cancer, pp 225–227
20. Purysko AS, et al. (2012) LI-RADS: a case-based review of the new categorization of liver findings in patients with end-stage liver disease. Radiographics 32(7):1977–1995
21. Goodman ZD (2007) Neoplasms of the liver. Mod Pathol 20:S49–S60
22. Nakanuma Y, et al. (2010) Pathological classification of intrahepatic cholangiocarcinoma based on a new concept. World J Hepatol 2(12):419–427
23. Akiba J, et al. (2013) Clinicopathologic analysis of combined hepatocellular-cholangiocarcinoma according to the latest WHO classification. Am J Surg Pathol 37(4):496–505
24. Kassahun WT, Hauss J (2008) Management of combined hepatocellular and cholangiocarcinoma. Int J Clin Pract 62(8):1271–1278
25. Yang JD, et al. (2011) Factors that affect risk for hepatocellular carcinoma and effects of surveillance. Clin Gastroenterol Hepatol 9(7):617–623
26. Sempoux C, et al. (2011) Intrahepatic cholangiocarcinoma: new insights in pathology. Semin Liver Dis 31(1):49–60
27. de Groen PC, et al. (1999) Biliary tract cancers. N Engl J Med 341(18):1368–1378
28. Xu J, et al. (2016) Combined hepatocellular-cholangiocarcinoma (cholangiolocellular type) with stem-cell features: a clinicopathologic analysis of 26 cases. Zhonghua Bing Li Xue Za Zhi 45(3):175–179
29. Zhang F, et al. (2008) Combined hepatocellular cholangiocarcinoma originating from hepatic progenitor cells: immunohistochemical and double-fluorescence immunostaining evidence. Histopathology 52(2):224–232
30. Bellissimo F, et al. (2015) Diagnostic and therapeutic management of hepatocellular carcinoma. World J Gastroenterol 21(42):12003–12021
31. Allaire GS, et al. (1988) Bile duct adenoma. a study of 152 cases. Am J Surg Pathol 12(9):708–715
32. Maximin S, et al. (2014) Current update on combined hepatocellular-cholangiocarcinoma. Eur J Radiol Open 1:40–48
33. Aoki K, et al. (1993) Combined hepatocellular carcinoma and cholangiocarcinoma: clinical features and computed tomographic findings. Hepatology 18(5):1090–1095
34. Chen LD, et al. (2010) Intrahepatic cholangiocarcinoma and hepatocellular carcinoma: differential diagnosis with contrast-enhanced ultrasound. Eur Radiol 20(3):743–753
35. Leoni S, et al. (2010) The impact of vascular and nonvascular findings on the noninvasive diagnosis of small hepatocellular carcinoma based on the EASL and AASLD criteria. Am J Gastroenterol 105(3):599–609
36. Sherman M (2010) The radiological diagnosis of hepatocellular carcinoma. In: Am J Gastroenterol. United States. p 610–612.
37. Ros PR, et al. (1986) Mesenchymal hamartoma of the liver: radiologic-pathologic correlation. Radiology 158(3):619–624
38. Kim KA, et al. (2006) Unusual mesenchymal liver tumors in adults: radiologic-pathologic correlation. AJR Am J Roentgenol 187(5):W481–W489
39. Lai FM, et al. (1996) Hepatic mesenchymal hamartoma: a case report and radiological findings. Singap Med J 37(2):226–228
40. Horton KM, et al. (1999) CT and MR imaging of benign hepatic and biliary tumors. Radiographics. doi:10.1148/radiographics.19.2.g99mr04431
41. Ros PR, et al. (1986) Mesenchymal hamartoma of the liver: radiologic-pathologic correlation. Radiology. doi:10.1148/radiology.158.3.3511498
42. Kim SH, et al. (2007) Radiological spectrum of hepatic mesenchymal hamartoma in children. Korean J Radiol 8(6):498–505
43. Cornette J, et al. (2009) Mesenchymal hamartoma of the liver: a benign tumor with deceptive prognosis in the perinatal period. Case report and review of the literature. Fetal Diagn Ther 25(2):196–202
44. Anil G, Fortier M, Low Y (1001) Cystic hepatic mesenchymal hamartoma: the role of radiology in diagnosis and perioperative management. Br J Radiol 2011(84):e91–e94
45. Isaacs H Jr (2007) Fetal and neonatal hepatic tumors. J Pediatr Surg 42(11):1797–1803
46. Lall C, et al. (2015) Renal collision and composite tumors: imaging and pathophysiology. Urology 86(6):1159–1164
47. Lopez-Beltran A, et al. (2006) 2004 WHO classification of the renal tumors of the adults. Eur Urol 49(5):798–805
48. Waldert M, et al. (2010) Hybrid renal cell carcinomas containing histopathologic features of chromophobe renal cell carcinomas and oncocytomas have excellent oncologic outcomes. Eur Urol 57(4):661–665
49. Su D, Singer EA, Srinivasan R (2015) Molecular pathways in renal cell carcinoma: recent advances in genetics and molecular biology. Curr Opin Oncol 27(3):217–223
50. Mucciardi G, et al. (2015) Transitional cell carcinoma of the renal pelvis with synchronous ipsilateral papillary renal cell carcinoma: case report and review. Urol Case Rep 3(4):93–95
51. Upton MP, et al. (2005) Histologic predictors of renal cell carcinoma response to interleukin-2-based therapy. J Immunother 28(5):488–495
52. Escudier B, et al. (2007) Sorafenib in advanced clear-cell renal-cell carcinoma. N Engl J Med 356(2):125–134
53. Polascik TJ, Bostwick DG, Cairns P (2002) Molecular genetics and histopathologic features of adult distal nephron tumors. Urology 60(6):941–946
54. Sukosd F, et al. (2003) Deletion of chromosome 3p14.2-p25 involving the VHL and FHIT genes in conventional renal cell carcinoma. Cancer Res 63(2):455–457
55. Gurel S, et al. (2013) Subtypes of renal cell carcinoma: MRI and pathological features. Diagn Interv Radiol 19(4):304–311
56. Sun MR, et al. (2009) Renal cell carcinoma: dynamic contrast-enhanced MR imaging for differentiation of tumor subtypes–correlation with pathologic findings. Radiology 250(3):793–802
57. Vargas HA, et al. (2012) Renal cortical tumors: use of multiphasic contrast-enhanced MR imaging to differentiate benign and malignant histologic subtypes. Radiology 264(3):779–788
58. Gordetsky J, Zarzour J (2016) Correlating preoperative imaging with histologic subtypes of renal cell carcinoma and common mimickers. Curr Urol Rep 17(7):52
59. Campbell N, Rosenkrantz AB, Pedrosa I (2014) MRI phenotype in renal cancer: is it clinically relevant? Top Magn Reson Imaging 23(2):95–115
60. Davidson AJ, et al. (1993) Renal oncocytoma and carcinoma: failure of differentiation with CT. Radiology 186(3):693–696
61. Rosenkrantz AB, et al. (2010) MRI features of renal oncocytoma and chromophobe renal cell carcinoma. AJR Am J Roentgenol 195(6):W421–W427
62. Perez-Ordonez B, et al. (1997) Renal oncocytoma: a clinicopathologic study of 70 cases. Am J Surg Pathol 21(8):871–883
63. Harmon WJ, King BF, Lieber MM (1996) Renal oncocytoma: magnetic resonance imaging characteristics. J Urol 155(3):863–867
64. Rosenkrantz AB, et al. (2010) Utility of the apparent diffusion coefficient for distinguishing clear cell renal cell carcinoma of low and high nuclear grade. AJR Am J Roentgenol 195(5):W344–W351
65. Taouli B, et al. (2009) Renal lesions: characterization with diffusion-weighted imaging versus contrast-enhanced MR imaging. Radiology 251(2):398–407
66. Mugiya S, et al. (2004) Ultrasonographic features of chromophobe cell renal carcinoma. Hinyokika Kiyo 50(12):865–868
67. Kondo T, et al. (2004) Spoke-wheel-like enhancement as an important imaging finding of chromophobe cell renal carcinoma: a

retrospective analysis on computed tomography and magnetic resonance imaging studies. Int J Urol 11(10):817–824
68. Shuch B, et al. (2012) Sarcomatoid renal cell carcinoma: a comprehensive review of the biology and current treatment strategies. Oncologist 17(1):46–54
69. de Peralta-Venturina M, et al. (2001) Sarcomatoid differentiation in renal cell carcinoma: a study of 101 cases. Am J Surg Pathol 25(3):275–284
70. Cheville JC, et al. (2004) Sarcomatoid renal cell carcinoma: an examination of underlying histologic subtype and an analysis of associations with patient outcome. Am J Surg Pathol 28(4):435–441
71. Shuch B, et al. (2009) Cytoreductive nephrectomy for kidney cancer with sarcomatoid histology–is up-front resection indicated and if not, is it avoidable? J Urol 182(5):2164–2171
72. Schieda N, et al. (2015) Diagnosis of sarcomatoid renal cell carcinoma with CT: evaluation by qualitative imaging features and texture analysis. AJR Am J Roentgenol 204(5):1013–1023
73. Sant GR, et al. (1984) Computed tomographic findings in renal angiomyolipoma: an histologic correlation. Urology 24(3):293–296
74. Kloos RT, et al. (1995) Incidentally discovered adrenal masses. Endocr Rev 16(4):460–484
75. Katabathina VS, et al. (2013) Adrenal collision tumors and their mimics: multimodality imaging findings. Cancer Imaging 13(4):602–610
76. Ctvrtlik F, et al. (2009) Differential diagnosis of incidentally detected adrenal masses revealed on routine abdominal CT. Eur J Radiol 69(2):243–252
77. Johnson PT, Horton KM, Fishman EK (2009) Adrenal mass imaging with multidetector CT: pathologic conditions, pearls, and pitfalls. Radiographics 29(5):1333–1351
78. Otal P, et al. (1999) Imaging features of uncommon adrenal masses with histopathologic correlation. Radiographics 19(3):569–581
79. Johnson PT, Horton KM, Fishman EK (2009) Adrenal imaging with multidetector CT: evidence-based protocol optimization and interpretative practice. Radiographics 29(5):1319–1331
80. Piotrowski Z, et al. (2015) Renal cell carcinoma and an incidental adrenal lesion: adrenal collision tumors. Urology 85(3):e17–e18
81. Reznek RH, Armstrong P (1994) The adrenal gland. Clin Endocrinol 40(5):561–576
82. Szolar DH, Kammerhuber F (1997) Quantitative CT evaluation of adrenal gland masses: a step forward in the differentiation between adenomas and nonadenomas? Radiology 202(2):517–521